A Zebrafish Model for a Human Myopathy Associated with Mutation of the Unconventional Myosin MYO18B

Ritika Gurung,*,[1] Yosuke Ono,[†,‡,1] Sarah Baxendale,[§,1] Samantha Lin Chiou Lee,* Steven Moore,[§] Meredith Calvert, and Philip W. Ingham*,[†,‡,§,2]**

*A*STAR Institute of Molecular and Cell Biology, Singapore 138673, Singapore, [†]Lee Kong Chian School of Medicine, Nanyang Technological University, Singapore 639798, Singapore, [‡]The Living Systems Institute, University of Exeter, EX4 4QD UK, [§]Department of Biomedical Science, University of Sheffield, S10 2TN, UK, and **Temasek Lifesciences Laboratory, Singapore 117604, Singapore

ORCID ID: 0000-0001-8224-9958 (P.W.I.)

ABSTRACT Myosin 18B is an unconventional myosin that has been implicated in tumor progression in humans. In addition, loss-of-function mutations of the *MYO18B* gene have recently been identified in several patients exhibiting symptoms of nemaline myopathy. In mouse, mutation of *Myo18B* results in early developmental arrest associated with cardiomyopathy, precluding analysis of its effects on skeletal muscle development. The zebrafish, *frozen* (*fro*) mutant was identified as one of a group of immotile mutants in the 1996 Tübingen genetic screen. Mutant embryos display a loss of birefringency in their skeletal muscle, indicative of disrupted sarcomeric organization. Using meiotic mapping, we localized the *fro* locus to the previously unannotated zebrafish *myo18b* gene, the product of which shares close to 50% identity with its human ortholog. Transcription of *myo18b* is restricted to fast-twitch myocytes in the zebrafish embryo; consistent with this, *fro* mutant embryos exhibit defects specifically in their fast-twitch skeletal muscles. We show that sarcomeric assembly is blocked at an early stage in *fro* mutants, leading to the disorganized accumulation of actin, myosin, and α-actinin and a complete loss of myofibrillar organization in fast-twitch muscles.

KEYWORDS MYO18B; nemaline myopathy; fast-twitch muscle; *frozen*; zebrafish

MYOSINS comprise a superfamily of actin driven motor proteins; although primarily known for their involvement in muscle contraction, many additional functions have been attributed to them, ranging from cell adhesion and polarity (reviewed by Vicente-Manzanares *et al.* 2009) to intracellular vesicular trafficking (reviewed by Akhmanova and Hammer 2010) and transcription (Philimonenko *et al.* 2004; Vreugde *et al.* 2006). Based on sequence comparisons of their conserved motor domain, the eukaryotic myosins have been assigned to ~35 phylogenetic classes (Odronitz and Kollmar 2007; Heissler and Sellers 2016). Two different types of myosin can be distinguished: conventional, which refers to all muscle myosins as well as nonmuscle myosins (belonging to Class II) that resemble them in their ability to associate into filaments; and unconventional, which refers to all other myosins. Among the latter type, members of six classes have been found to be expressed in muscle (Redowicz 2007).

The unconventional myosin MYO18B is encoded by a gene originally identified by sequence annotation of human chromosome 22 and shown to share ~40% sequence identity with the previously described *MYO18A* gene (Berg *et al.* 2001). Subsequent human genetic studies identified *MYO18B* as a tumor suppressor gene, based on its deletion in a lung carcinoma cell line and in 60% of all lung cancers assayed (Nishioka *et al.* 2002). In an independent study, *MYO18B* was identified in a human skeletal muscle complementary DNA (cDNA) library and found to be expressed in human cardiac muscle and testes, as well as in skeletal muscle (Nishioka *et al.* 2002; Salamon *et al.* 2003). Analyses of *Myo18B* expression in the mouse are consistent with a role in the development and maintenance of both cardiac and skeletal muscle. A *Myo18B:LacZ* reporter gene is expressed in both the

doi: 10.1534/genetics.116.192864
Manuscript received June 20, 2016; accepted for publication November 18, 2016; published Early Online November 21, 2016.
Supplemental material is available online at www.genetics.org/lookup/suppl/doi:10.1534/genetics.116.192864/-/DC1.
[1]These authors contributed equally to this work.0002
[2]Corresponding author: Lee Kong Chian School of Medicine, Nanyang Technological University, 50 Nanyang Ave., Singapore 639798, Singapore. E-mail: pingham@ntu.edu.sg

myotome and heart in the developing mouse embryo, (Ajima *et al.* 2008) while in C2C12 cells, *Myo18B* is expressed at a basal level in undifferentiated myoblasts and upregulated upon their differentiation into myofibers (Salamon *et al.* 2003).

Two recent studies have associated mutations of human *MYO18B* with nemaline myopathy. In the first of these, two patients with Klippel-Feil anomaly (KFA) were found to be homozygous for a nonsense mutation in the penultimate exon of the *MYO18B* gene (Alazami *et al.* 2015); notably, both patients exhibited symptoms of myopathy (hypotonia and muscle weakness), a condition not previously associated with KFA. Muscle biopsy analysis of one patient revealed variation in fiber size and a loss of normal banding indicative of a loss of thick filaments. Electron microscopy (EM) analysis also revealed scattered, dense bodies reminiscent of nemaline rods, typical of other human myopathies (Wallgren-Pettersson *et al.* 2011). In a second study, a single infant with severe axial and peripheral hypotonia, who died at 4 months, was found to be homozygous for a premature termination codon in the last exon of the *MYO18B* gene. Muscle biopsies from this individual revealed variation in fiber size as well as small nemaline rods (Malfatti *et al.* 2015).

In contrast to the postnatal survival of the KFA patients, reverse genetic studies have revealed *Myo18B* to be essential for normal embryonic development in the mouse (Ajima *et al.* 2008). Embryos homozygous for a targeted knockout of the locus die of cardiac defects by E10.5 and show disrupted myofibrils in their cardiomyocytes, the thick and thin filaments of the sarcomere appearing misaligned. This early embryonic lethality and growth retardation of mutant embryos, however, precluded analysis of Myo18B function in skeletal muscles.

Forward genetic screens for mutations affecting muscle development and function in the zebrafish yielded a number of mutants including *frozen* (*fro*) and *sloth*, originally identified on the basis of their complete lack of motility (Granato *et al.* 1996). Morphological analysis of *sloth* and *fro* embryos revealed an absence of striated muscle fibers and a failure of muscle cell nuclei to elongate, suggestive of an early block in their differentiation (Granato *et al.* 1996). Molecular characterization of the *sloth* locus showed the phenotype to be due to a loss-of-function mutation in the *hsp90A* gene, implicating the chaperone protein that it encodes in myofibril formation (Hawkins *et al.* 2008). Here, we show that the *fro* mutant phenotype is caused by loss-of-function of the zebrafish *myo18b* gene. Our analysis reveals that *myo18b* is expressed specifically in precursors of fast-twitch skeletal muscle fibers, in which it is required for the assembly of myofibrils.

Materials and Methods

Zebrafish and husbandry

Zebrafish were raised, bred, and staged following standard methods (Kimmel *et al.* 1995). Developmental stages are annotated as hours postfertilization (hpf) or days postfertilization (dpf). Wild-type embryos were obtained from the AB strain. The fro^{to27c} mutation that was isolated in a large-scale chemical mutagenesis screen at the Max-Planck Institute für Entwicklungsbiologie (Granato *et al.* 1996) was maintained in the AB genetic background and outcrossed to the polymorphic WIK (L11) strain of wild-type fish to generate mapping embryos for positional cloning. The $Tg(smyhc1{:}GFP)^{i104}$ transgenic line has been previously described (Elworthy *et al.* 2008). Fish were maintained and manipulated in the University of Sheffield and the Institute of Molecular and Cell Biology (IMCB) zebrafish facilities in compliance with the UK Animals (Scientific Procedures) Act 1986 or the Biomedical Research Council (BMRC) Institutional Animal Care and Use Committee (IACUC) guidelines, respectively.

Induction of new fro/myo18b mutant alleles

ENU mutagenesis: Adult wild-type (AB) male zebrafish were mutagenized using ENU according to an improved mutagenesis protocol (Kettleborough *et al.* 2011). The G0 mutagenized individuals were outcrossed to wild-type females and the resultant F1 males test-crossed to females heterozygous for the fro^{to27c} allele. Each cross was screened for immotile progeny and a single male segregating an allele that failed to complement the fro^{to27c} allele was identified. The allele transmitted by this male was designated fro^{i230}.

Clustered regularly interspaced short palindromic repeats (CRISPR)/Cas9 mutagenesis: A target sequence in exon 3 of the *myo18b* gene (5′-GGCCGAGATGTCGCTGCGAG-3′) was identified using ZiFiT Targeter software (http://zifit.partners.org/ZiFiT/) and the sequence inserted into the *Bsa*I site of pDR274 guide RNA (gRNA) expression vector (Hwang *et al.* 2013). To synthesize gRNA, the template DNA fragment was amplified from the vector using the primer pair (forward: 5′-CATTATGGTGAAAGTTGGAAC-3′ and reverse: 5′-AAAAGCACCGACTCGGTGCCAC-3′), and gRNA was transcribed using a MEGAshortscript T7 Kit (Invitrogen, Carlsbad, CA) following the manufacturer's instructions. gRNA was injected into fertilized eggs at 100 ng/μl together with codon-optimized Cas9 messenger RNA (mRNA) with nuclear localization signals at 150 ng/μl. The Cas9 mRNA was synthesized from the pCS2-nCas9n vector (Jao *et al.* 2013). Injected embryos were raised to adults and F1 embryos screened for targeted mutations using the primer pair (forward: 5′-CCAGCAAACTCAGCGACAACCTA-3′ and reverse: 5′-CTGCAGGTCTGTGTTTCTGC-3′) to amplify the target locus and sequence for genotyping.

Positional cloning of the fro locus

Simple sequence length polymorphisms that flanked the *fro* locus, *z21976* and *z3260*, were used to identify 69 and 21 recombinants, respectively, from 1774 meioses, as previously described (Talbot and Schier 1999). The full-length coding sequence of zebrafish *myo18b* was deduced from four ESTs (LOC100537963, ENDSTART00000122824,

ENDSTAR00000124853, and ENDSTAR000001249931) that align well to the human MYO18B coding sequence. ENDSTAR000001249931 aligns to the 3′ end of the coding sequence (CDS) and contains the stop codon. The full-length coding sequence of *myo18b* was cloned in two separate overlapping fragments. Total cDNA prepared from 48 hpf embryos was used to clone the full-length sequence. Primer pair Fragment-I Forward: 5′-TTTGCTTCTCCTGGTCTCGT-3′ and Fragment-I Reverse: 5′-CTGCTCCACACGACTCTGTA-3′, was used to amplify the first half (3369 bp), and Fragment-II Forward: 5′-GGAGAAGGAGCGAAACGAGT-3′ and Fragment-II Reverse: 5′-TGTGCTTCCAGTTAAACGCA-3′ primer pair was used to amplify the second half (3121 bp) of the cDNA. Both the fragments were cloned into the pGEMT-Easy vector first. The *Hin*dIII restriction enzyme site at 3302 bp from the translational start site, which included in both fragments, was used as the junction for cutting and ligating the two cloned halves of the DNA, removing 187 bp of overlapping region. The 6303 bp, full-length, myo18B CDS in pGEMT-*myo18b* (FL) plasmid was *Sph*I/*Spe*I-digested for cloning into the pCS2(+) expression vector for *in vitro* transcription. The cloned *myo18b* CDS was sequenced with 17 overlapping primers to validate the sequences.

RT-PCR and semiquantitative real-time PCR

Total RNA was isolated from zebrafish embryos using Trizol reagent (Invitrogen), according to the manufacturer's instructions. Total RNA was synthesized into cDNA using random oligo$(dT)_{12–18}$ primers and Superscript III reverse transcriptase (Invitrogen).

DNA constructs

Full-length zebrafish *myo18b* was amplified from 24 hpf and 48 hpf cDNA and cloned into pCS2 vectors *in vitro* transcription (Ambion).

In situ probes: These were constructed by cloning 5′and 3′ region amplified by primers:

5′18B_ISM_F4 - 5′-CTGGTCGGGATCTTCTGCTT-3′(Forward)
5′18B_ISM_R4 - 5′-AGACAGCACCATGGCGAATC-3′(Reverse)
ism_3′probe_F - 5′-AAAGTTCTGGAGGTCTCGGG-3′ (Forward)
ism_3′probe_R - 5′-TTCCGACATGCTCTGCTTTG-3′ (Reverse)

into pGEMT vectors. The plasmids were linearized and *in vitro* transcribed using the T7 polymerase (Ambion) for 3 hr. Probes were used at a concentration of 10 ng/μl and incubated at 72° for hybridization.

sox6:lifeact-gfp: The coding sequence of the Lifeact-GFP fusion protein (Riedl *et al.* 2008) was cloned downstream of the fast-twitch fiber-specific 5.7 kb promoter of the *sox6* gene (Wang *et al.* 2011) in pDestTol2pA2 backbone vector using the Gateway cloning system (Invitrogen). Transient expression of Lifeact-GFP, to visualize actin filaments in muscle fibers, was achieved by injecting ~1 nl of a 50 ng/μl DNA solution into one-cell stage embryos.

Whole mount in situ hybridization and immunofluorescence

Whole mount *in situ* hybridization (WISH) and immunofluorescence was performed essentially as previously described (Wang *et al.* 2011). Embryos were fixed in 4% paraformaldehyde prior to processing for WISH or incubation with antibodies. Primary antibodies used were as follows: mouse mAb anti-α-Actinin (EA-53 Abcam, 1:600); mouse mAb anti-dystrophin MANDRA1 (DSHB, 1:150); mouse mAb F310 (DSHB, 1:50); rabbit anti-GFP (Torrey Pines, 1:2500); rabbit anti-Laminin (L9393 Sigma [Sigma Chemical], St. Louis, MO, 1:500); rabbit anti-thrombospondin-4b (Subramanian and Schilling 2014) (kind gift of T. Schilling, 1:500) Secondary antibodies used were: anti-mouse Alexa Fluor 546 (Molecular Probes, Eugene, OR, 1:850) and anti-rabbit Alexa Fluor 488 (Molecular Probes, 1:2500). Nuclei were visualized using DAPI (4',6-diamidino-2-phenylindole dihydrochloride, 1:2000, Molecular Probes). Actin was visualized using Phalloidin Tetramethylrhodamine B isothiocyanate (Sigma) (1:300 dilution of a 2.5 μg/μl DMSO stock solution). Imaging used a Zeiss ([Carl Zeiss], Thornwood, NY) LSM 510 confocal microscope with ImageJ software.

Transmission electron microscopy (TEM)

48 hpf embryos were fixed in 4% paraformaldehyde and 0.5% glutaraldehyde in 0.1 M sodium cacodylate buffer, postfixed in 1% osmium tetroxide, dehydrated through an ethanol series and embedded in Spurr's resin. Images were captured on a JEOL JEM-1230 transmission electron microscope equipped with a 4 k × 4 k Gatan Orius CCD camera. Figures were assembled using Adobe Photoshop CS3 Extended.

Data availability

The authors state that all data necessary for confirming the conclusions presented in the article are represented fully within the article.

Results

fro mutants lack skeletal muscle activity, and have disorganized myofibrils and cardiac defects

Homozygous fro^{to27c} mutant embryos can be identified at approximately 24 hpf when their wild-type siblings commence spontaneous muscle contraction; the mutants, by contrast, responding only to tactile stimuli with slight spasms (Supplemental Material, File S1 and File S2). This phenotype appears fully penetrant and recessive, based on the proportion of mutant embryos observed in the progeny of in-crosses between heterozygous parents (see Table 1). As originally described (Granato *et al.* 1996), homozygous fro^{to27c} embryos displayed an almost complete loss of birefringency, a manifestation of the rotation of polarized light caused by sarcomeric repeats, compared to their wild-type siblings, indicating defects in the organization of the sarcomeric

structures (Figure 1, A–D). The fast-twitch fibers in the trunk and tail muscles of *fro*^{to27c} mutant embryos lacked the typical striated distribution of α-actinin, which instead formed large aggregates (red; Figure 1, E and G). Myosin heavy chain protein accumulated throughout the fast-twitch fibers of *fro*^{to27c} mutant embryos, in contrast to the ordered myofibrillar distribution typical of wild-type fibers (Figure 1, F and H). TEM analysis of trunk muscles revealed that the tightly packed ordered arrays of thin and thick filaments visible in transverse sections of wild-type fibers were largely absent from *fro*^{to27c} mutant fibers (Figure 1, I and K). Consistent with the disruption of α-actinin distribution, I-Z-I boundaries, clearly visible as vertical lines in wild-type muscle fibers (Figure 1J), were completely missing in *fro*^{to27c} mutant embryos (Figure 1L).

By contrast to the fast-twitch fibers, α-actinin staining revealed a striated pattern in the slow-twitch fibers similar to that of their wild-type counterparts (Figure 1, N and P). As development proceeded, the slow-twitch fibers became less well-aligned, but retained their striated pattern (Figure S1). Most craniofacial muscles are comprised of both slow-twitch fibers and fast-twitch fibers (Hernandez *et al.* 2005). In *fro*^{to27c} mutant larvae, the striated distribution of α-actinin was unaffected in the former but disrupted in the latter, the protein accumulating in large amorphous "blobs" (Figure 1, M and O).

At 48 hpf, *fro*^{to27c} mutants displayed spasms or exhibited no response to touch stimulus, and by 72 hpf they were completely immotile. By this stage, mutant larvae had enlarged underutilized yolks and slightly curved spines (data not shown). Mutant larvae also had an enlarged pericardium and a dilated atrium (Figure S2, A and B) and exhibited reduced blood circulation with pooling of blood in the pericardial cavity (Figure S2B). The heart rate of *fro*^{to27c} mutants, however, was not significantly different from wild-type animals at 48 hpf (Figure S2C). Immunostaining with anti α-actinin revealed the striation pattern of *fro* cardiomyocytes to be similar to that of wild-type (Figure S2, D–F).

The fro mutation maps to the myo18b gene

The *fro* mutation was originally rough-mapped to LG10 (R. Geisler, personal communication). To determine its precise location, SSLP markers *z21976* and *z3260* were used to identify 69 and 21 recombinant *fro* embryos, respectively, from 1774 meioses (Figure 2A). The closest marker, *z9701* (19 recombinants), mapped to the *mef2ca* gene, 1.07 cM from *fro*, while z3260 mapped to the *camk2b2* gene. The genetic distance between the two closest flanking markers corresponded to an estimated physical distance of 1.46 Mb, with *fro* close to the center. This correlates well with the distance of 1.39 Mb between *z9701* and *z3260* on the GRCz10 zebrafish genome assembly (https://www.ncbi.nlm.nih.gov/assembly/GCF_000002035.5/). The region between *mef2c* and *camk2b* shows a high degree of conserved synteny between zebrafish and tilapia, with many of the genes in this interval also showing conserved synteny in other fish species, including medaka *fugu*, and *tetraodon*. Notably, *adrbk2* is located close to the center of this region

Table 1 Segregation of the *fro* mutant phenotype among the progeny of in-crosses of mutant heterozygotes

	Phenotype			
Allele	Frozen	Wild-Type	Total	% Frozen
to27c	347	1039	1386	25.0
i230	360	1106	1466	24.6
i311	405	1201	1606	25.2
i310	82	233	315	26.0

Progeny were scored at 48 hpf for lack of motility, pericardial swelling, and blood pooling. For *fro*^{to27c} an equal number (48) of embryos scored as mutant or wild-type were genotyped by sequencing of the *myo18b* locus; all 48 of the mutants were found to be homozygous for the lesion associated with the *fro*^{to27c} allele, while phenotypically wild-type embryos were either heterozygous (33) or homozygous (15) for the wild-type allele.

in all five species and in four of them the gene adjacent to *adrbk2* is *myo18b* (Figure 2C), a syntenic relationship that is conserved in mammals (Nishioka *et al.* 2002). Although missing from this region in the GRCz10 assembly, we considered *myo18b* to be a good candidate for the *fro* gene, since it had appeared here in the previous GRCz9 assembly.

The full-length coding sequence of zebrafish *myo18b* was deduced from four ESTs that align well to the human *MYO18B* coding sequence, which has 2567 residues; the sequence has been deposited in GenBank with the accession number KX421389. Zebrafish *myo18b* cDNA has 52% identity with human *MYO18B*, while the predicted protein sequences share 47% identity (see Figure S3). The complete *myo18b* cDNA in zebrafish is encoded by 37 exons (Figure 3A), with a large genomic fragment containing ~27 exons of N-terminal coding region encompassing three ESTs aligning within one fragment, and another EST encoding the C-terminal region forming a second fragment separated by a 250 kb intervening region. BLAST analysis of the *myo18b* cDNA sequence revealed it to derive from a locus adjacent to *adrbk2*, as in other species (see Figure 2). The locus is within the final 1.5 Mb at the end of the chromosome and the *myo18b* gene sequence is distributed across several fragments in GRCz10, with one fragment placed further toward the telomere (LOC100331349) and two large fragments from the 5′ (LOC100537963) and 3′ (LOC10033206) ends of the gene in the correct location (Figure 2B). This fragmentation of the gene is likely to be due to errors in the sequence assembly in the subtelomeric region, something that has been observed for other chromosomes, for example in the course of cloning the *cloche* gene (Reischauer *et al.* 2016). The *myo18b* locus is also fragmented in the genome assemblies of several other fish species, with many incomplete transcripts aligning within this genomic region.

Sequencing of cDNAs from 48 hpf wild-type (AB) embryos and from embryos homozygous for *fro*^{to27c} or *fro*^{i230}, a second ENU-induced mutant allele isolated on the basis of its non-complementation of *fro*^{to27c} (see *Materials and Methods*), identified lesions in the transcribed region of *myo18b* in both mutant alleles (Figure 3, A and B). The corresponding single-base substitutions were detected in the genomic DNA from

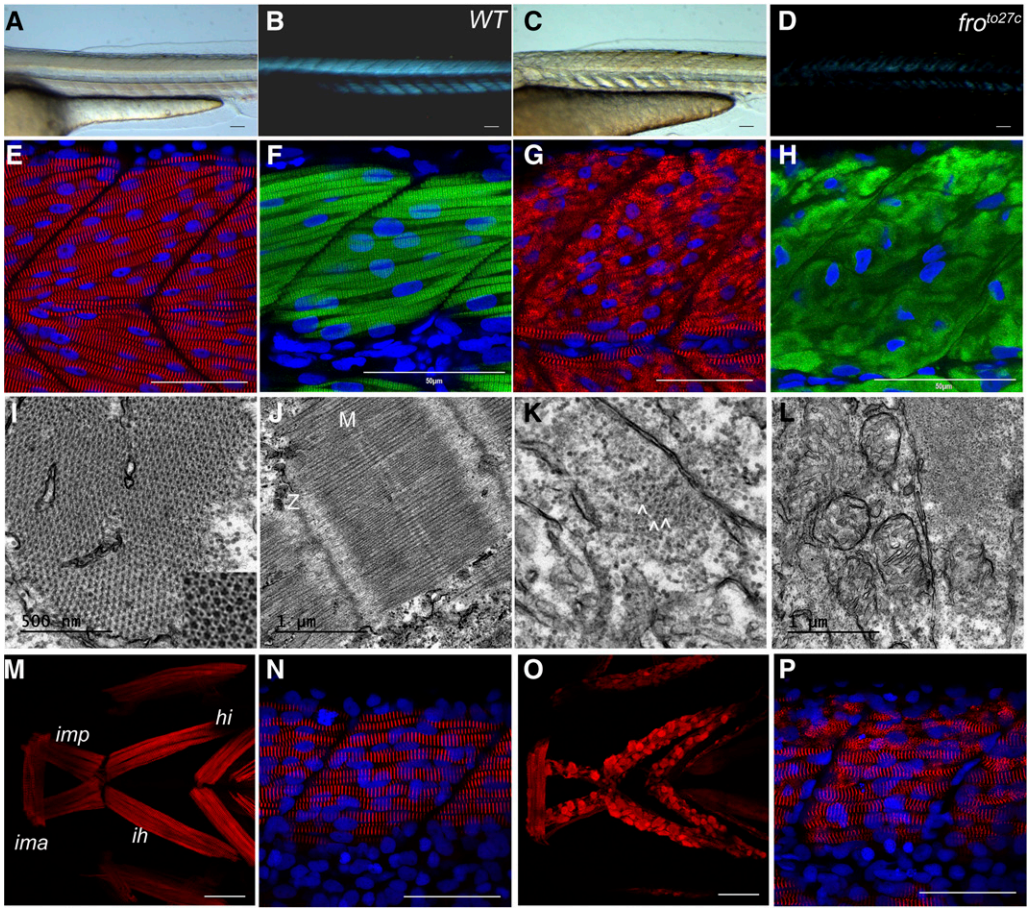

Figure 1 *frozen* mutants have disorganized fast-twitch skeletal muscle fibers. (A–D) Brightfield (A and C) and polarized (B and D) illumination images of the trunk region of wild-type (WT) (A and B) and *fro*^{to27c} mutant (C and D) embryos at 36 hpf (hours postfertilization), showing loss of birefringence in the mutant. Bar, 50 μm. (E–H) Distribution of α-actinin (red) or myosin heavy chain (mAb310; green) in the fast-twitch muscle fibers of 48 hpf wild-type (E and F) and *fro*^{to27c} (G and H) embryos; note the absence of striated myofibrils and the amorphous accumulation of both sarcomeric proteins in the mutant embryos. Nuclei are stained blue (DAPI). Scale bar in all panels, 50 μm. (I–L) Transmission electron micrographs of transverse and sagittal sections of skeletal muscle fibers from the trunk region of wild-type (I and J) and *fro*^{to27c} mutant (K and L) embryos fixed at 48 hpf. Transverse sections show the ordered arrays of thick and thin filaments in a wild-type muscle fiber (I); the regular lattice-like arrangement of thin filaments surrounding each thick filament is shown at higher magnification in the inset. This organization was largely absent from mutant muscles although some residual filaments could be detected in some fibers (arrowheads) (K). Sagittal sections reveal the typical sarcomeric organization of a wild-type muscle fiber (J) with its characteristic Z-lines (Z) and M-lines (M). This organization is absent from *fro*^{to27c} mutant muscle (L), which is characterized instead by abnormally enlarged mitochondria. The enlarged mitochondria are more than twice the diameter of those in normal wild-types. (M and O) Distribution of α-actinin (red) in the intermandibularis anterior (IMA), Intermandibularis posterior (IMP), interhyoideus inferior (IH), and hyohyoideus inferior (HI) muscles in 5 dpf (days postfertilization) wild-type (M) and *fro*^{to27c} (O) mutant larvae; note the loss of striations and globular accumulation of α-actinin in many of the fibers in each muscle except the IMA, which is predominantly slow-twitch. (N and P) Distribution of α-actinin (red) in the slow-twitch muscle fibers of wild-type (N) and *fro*^{to27c} (P) embryos showing well-defined striations in the mutant. Nuclei are stained blue (DAPI). Scale bar in all light micrographs, 50 μm. Scale bars in transmission electron microscopy images as indicated; panel (K) is the same magnification as panel (I). All panels show single confocal planes except for (N) and (P), which are composed of stacks of 4 × 0.7 μm optical sections.

each mutant: *fro*^{to27c} is an A–G mutation in codon 1632 (Figure 3C) that falls within the coiled-coil tail domain of the protein (Figure 3B); it disrupts a splice acceptor site causing a deletion of 26 bp from exon 32 (Figure 3A). Primer pairs that amplify a 1.2 kb region of *myo18b* transcripts, including the *fro*^{to27c} mutation site, identified several shorter species in the cDNA from *fro*^{to27c} homozygous embryos (72 hpf), while in samples from heterozygous embryos the original band was also amplified (data not shown). These bands were not observed in cDNA from *fro*^{i230} homozygotes or heterozygotes. Genomic sequence analysis confirmed that *fro*^{i230} is a G–A point mutation in codon 698 (Figure 3D) that lies within the motor head domain of the protein (Figure 3B). Two splice forms of *myo18b* were identified when cDNA from *fro*^{i230} mutant was compared to wild-type, one with an inclusion of 118 bp from the intronic region and the other with 33 bp deletion from the exon. This results in a frameshift in case of the former, while the latter may form a truncated protein (data not shown).

To test whether complete loss-of-function of the *myo18b* gene is causative of the *fro* phenotype, the locus was targeted using CRISPR/Cas9-mediated mutagenesis (Hwang *et al.* 2013). Two alleles, designated *fro*^{i310} and *fro*^{i311}, encoding a 2 bp deletion and 7 bp deletion in exon 3, respectively, were isolated (Figure S4), both of which when homozygous resulted in motility defects similar to *fro*^{to27c} and *fro*^{i230} and failed to complement the immotile phenotype *in trans* to *fro*^{to27c}. Like the ENU-induced alleles, these CRISPR-induced alleles were found to be fully penetrant (Table 1); the expressivity of the myofibril phenotype in the *fro*^{i230} and *fro*^{i311}was slightly weaker than that of the other two alleles, both displaying evidence of limited myofibrillar organization in a small proportion of their fast-twitch fibers (Figure S4).

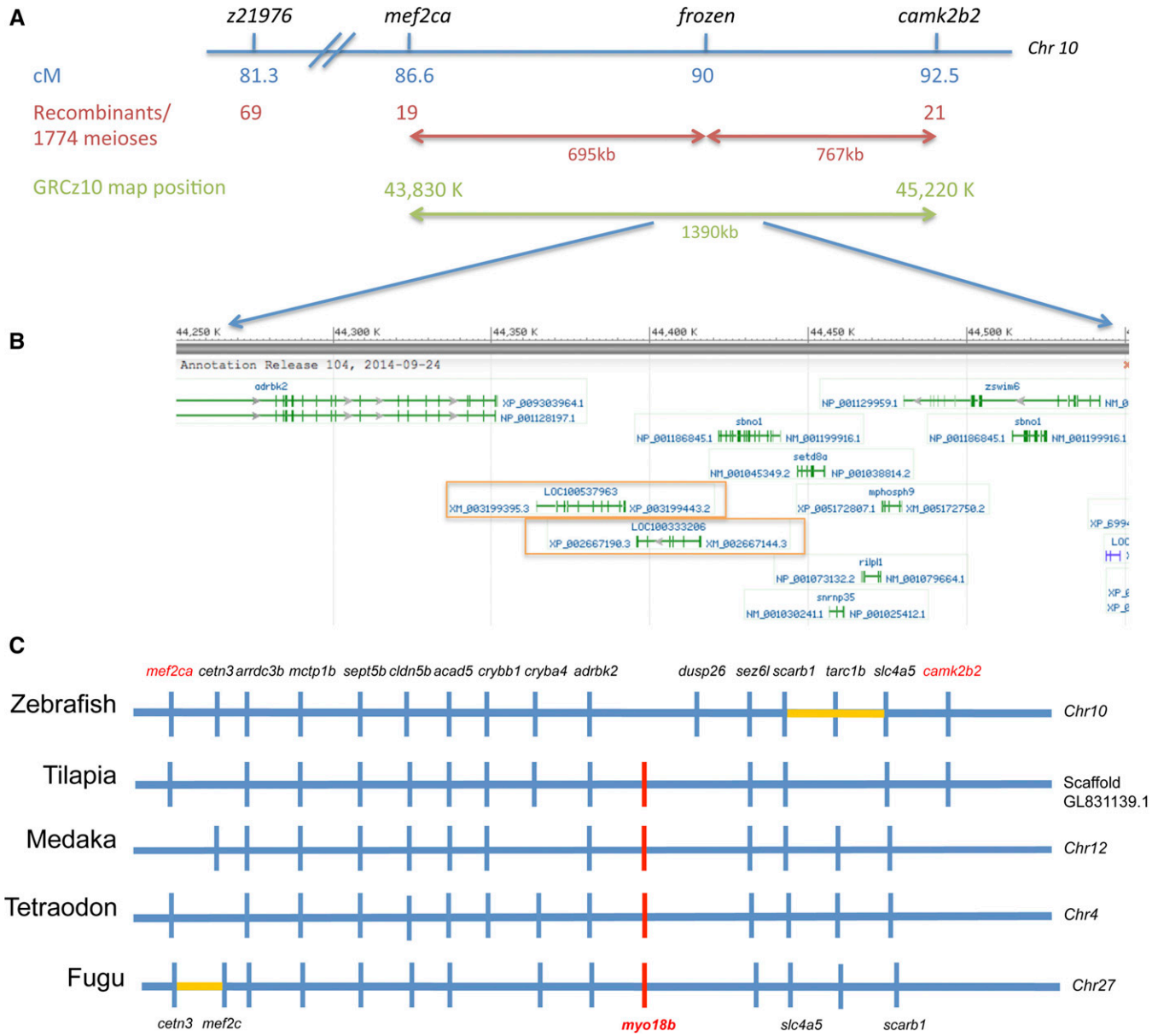

Figure 2 Mapping of the *frozen* locus. (A) Genetic map around *fro* on chromosome 10. The genetic distance on the MGH (Massachusetts General Hospital) genetic map Knapic *et al.* (1998) is shown in centimorgan, along with the number of recombinants in 1774 meioses obtained with flanking markers and the estimated distance between the closest flanking markers (red). The physical distance and position of the flanking markers on the latest genome assembly GRCz10 is shown in green. (B) The region of the GRCz10 genome assembly containing two fragments of the *myo18B* gene, LOC100537963 and LOC10033206, outlined in orange. (C) Comparative synteny of the region flanked by *mef2ca* and *camk2b2* in zebrafish and four other fish species. The *myo18b* gene is located immediately adjacent to the *adrbk2* locus in tilapia, medaka, and pufferfish (*Tetraodon* and *Fugu*), a relationship that is conserved in mammals, including human (not shown). Yellow horizontal lines indicate regions that are inverted relative to the arrangement in the majority of the fish species shown. Chr, chromosome.

myo18b is expressed in fast-twitch muscles of the developing zebrafish embryo

Expression of *myo18b* was first detected by RT-PCR at the 14 somite stage (Figure 4A), increasing in levels up to 5 dpf. Two probes complementary to the 5′ or 3′ end of the transcript were used for WISH analysis, such that most alternative splice forms would be detected. The 5′ probe that includes 40 bp from the UTR and the first 1200 bases of the transcript, and the 3′ probe that includes 368 bp of the 3′-UTR region, revealed identical patterns of expression at all embryonic stages. Consistent with the PCR analysis, expression was first observed in 10–14 somite stage embryos prior to the onset of muscle fiber differentiation, exclusively in the developing myotome (Figure 4B). High levels of *myo18b* transcript persisted in the muscles from 24 to 72 hpf, with transcripts localized preferentially to the somite boundaries. Transverse sections of *Tg(smyhc1:gfp)*^{i104} animals, which express GFP in their slow-twitch muscle fibers,

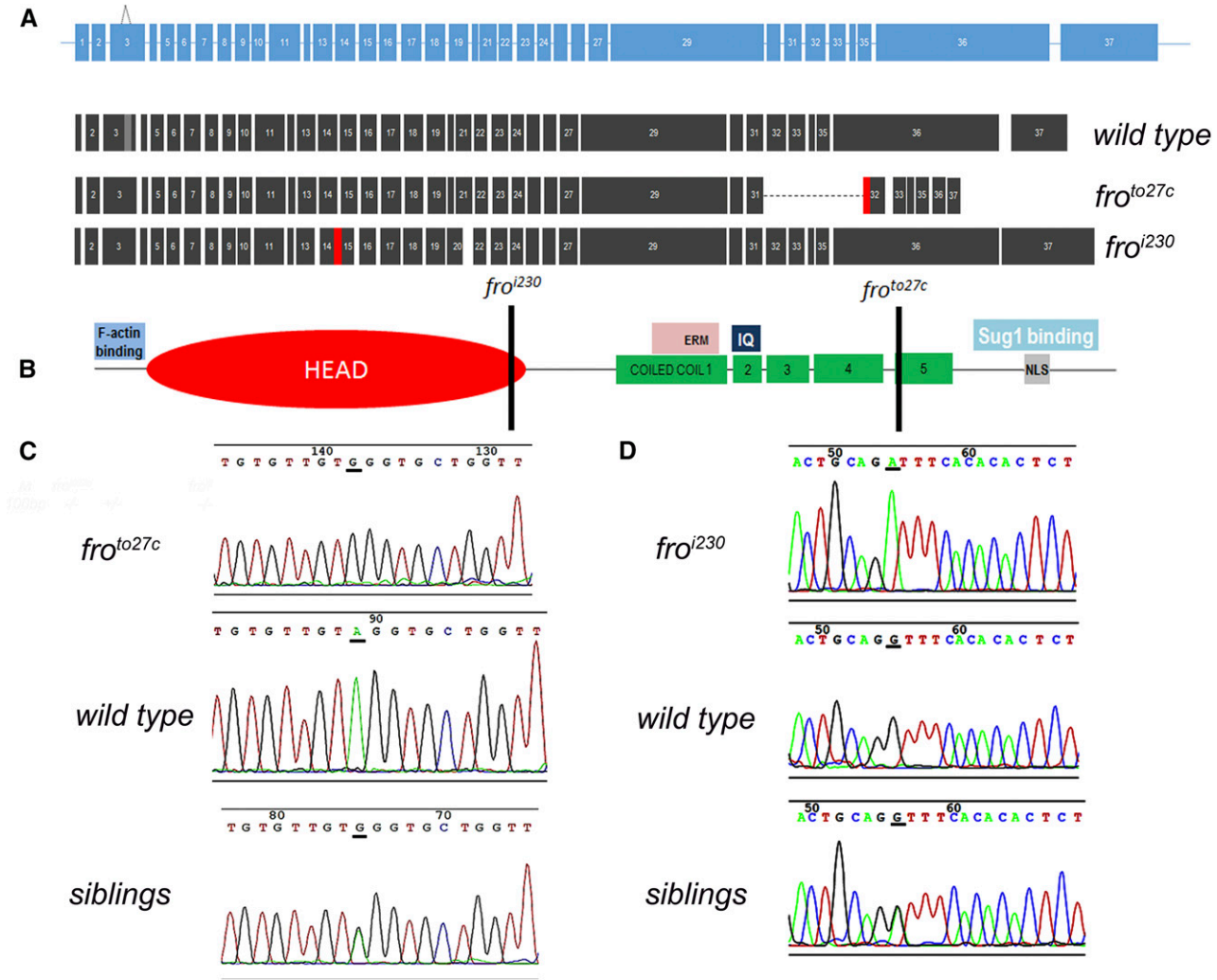

Figure 3 The *fro*^{to27c} and *fro*^{i230} mutant alleles disrupt the Myo18B protein. (A) Aligning the full-length *myo18b* complementary DNA to the human *MYO18B* coding sequence identified 37 exons (blue) that generate a transcript (black) 6303 bp after splicing. The *fro*^{to27c} mutation lies in codon 1632 while the *fro*^{i230} mutation is located in codon 698. The *fro*^{to27c} and *fro*^{i230} mutations may result in splicing defects (region marked by red) that in turn may lead to truncation of the mutant transcripts. (B) Myo18B has a typical myosin head domain (red) at its N-terminus, a coiled-coil tail domain (green), and a NLS at the C-terminal end. Colored boxes signify the binding sites for proteins or motifs as labeled. Solid black bars indicate the location of the mutated residues in the *fro* alleles. (C and D) DNA chromatograms showing the mutated sequences in *fro*^{to27c} and *fro*^{i230} homozygotes and the sequences of the same regions in wild-type and heterozygous siblings. The *fro*^{to27c} allele has an A–G transition mutation and the *fro*^{i230} allele, a G–A transition mutation. ERM, ezrin/radixin/moesin; IQ, calmodulin binding motif; NLS, nuclear localization signal.

hybridized with fluorescently-labeled *myo18b* probe revealed that the *myo18b* transcript accumulates exclusively in the fast-twitch fibers (Figure 4, D, F, and H). Expression of *myo18b* was detected in the developing heart tube at 24 hpf (Figure 4M), persisting at 48 hpf, when the heart develops into the two-lobed atrium and ventricle structure (Figure 4N). By 72 hpf, many jaw muscles and the optic muscle also showed robust *myo18b* expression (Figure 4L). Additionally, transcript was visible in the pectoral fin and hypaxial muscle, initially at 48 hpf (Figure 4K) and becoming well-defined by 72 hpf (Figure 4L).

The expression of *myo18b* was analyzed in *fro*^{to27c} and *fro*^{i230} homozygous mutant embryos by WISH. In both cases, the preferential accumulation of transcript at the somite boundaries typical of wild-type was absent, while transcript levels appeared lower in *fro*^{to27c} homozygotes than in *fro*^{i230} homozygotes or *fro*^{i230}/*fro*^{to27c} transheterozygotes (Figure S5). This suggests that the *fro*^{to27c} mutant transcript may be less stable than the wild-type form.

Myofibril assembly is blocked in fro mutants

To determine when during myofibrillogenesis Myo18B function is required, we compared the dynamics of myofibril assembly in wild-type and *fro*^{to27c} mutant embryos. To highlight actin filaments in individual muscle fibers, newly fertilized eggs were injected with a plasmid encoding Lifeact under the control of the *sox6* promoter, which drives expression in fast-twitch fibers (Wang *et al.* 2011), and the resulting embryos were fixed at various time-points and stained with anti-α-actinin antibody. As previously described (Kim and Ingham 2009), small punctate

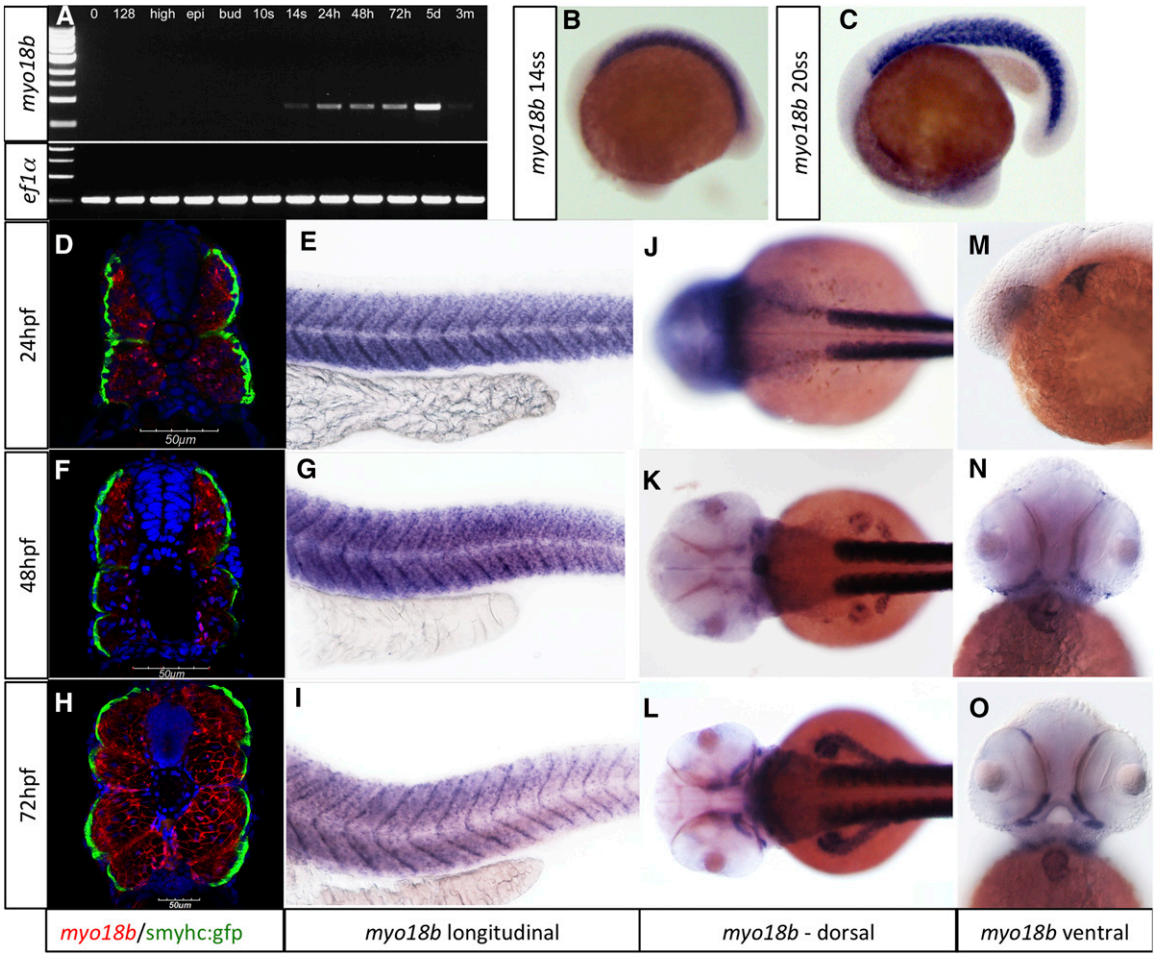

Figure 4 Expression of *myo18b* messenger RNA during embryonic development. (A) RT-PCR analysis of the *myo18b* transcript and *ef1*α reference control was performed on a range of developmental stages from fertilization to 3 months. Expression begins at 14 somite stage (ss) and increases up to 5 dpf (days postfertilization). (B–O) Detection of *myo18b* transcript by *in situ* hybridization. Transcript is first clearly detected at the 14 ss (B) and is restricted to the developing myotome. Transcript continues to accumulate in the myotome at the 20 ss (C). (D) Transverse sections through 24 hpf (hours postfertilization) *Tg(smyhc1:gfp)* embryos hybridized with fluorescently-labeled *myo18b* probe (red) show expression is restricted to the fast-twitch muscle fibers (nuclei are stained blue, DAPI); by this stage, there is increased accumulation of transcript at the somite boundaries (E). Transcript persists in fast-twitch fibers through 48 and 72 hpf (F–I). Transcript is first detectable in the pectoral fin and hypaxial muscle at 48 hpf (K) and is well-defined at 72 hpf (L). Transcript is detectable in the developing rudimentary heart tube by 24 hpf (M) and persists through 48 hpf (N) and 72 hpf (O). At 48 hpf, a few jaw muscles also accumulate transcript (K) and by 72 hpf transcript is present in more jaw and eye muscles (L and O).

beads of α-actinin were visible in regular arrays along the sarcolemma of fast-twitch myotubes in wild-type embryos at 24 hpf, when regular arrays of Z-line α-actinin were already visible along the medially located, slow-twitch muscle pioneer fibers (Figure 5, A and A'). In *fro*^{to27c} embryos at the same stage, α-actinin also accumulates in puncta but these are irregularly distributed in fast-twitch fibers (Figure 5, D and D'). In wild-type embryos, the regular punctate distribution of α-actinin along the sarcolemma was transformed into a regular repeating array of thin stripes, representing the Z-lines of the nascent myofibrils by 32 hpf (Figure 5B). By contrast, in *fro*^{to27c} embryos at the same stage, the distribution of α-actinin was relatively diffuse, accumulating throughout the cytoplasm of the muscle fibers (Figure 5E). By 48 hpf, the Z-lines extended linearly into wider bands that delineate each sarcomere in wild-type embryos (Figure 5C), interdigitating with the M-lines (Figure 5C'). In *fro*^{to27c} mutants, by contrast, α-actinin accumulated throughout the myotubes and showed no evidence of sarcomeric organization (Figure 5F). Individual fibers highlighted by the Lifeact labeling could be seen to span the full width of the somite in *fro*^{to27c} mutant embryos, showing no evidence of detachment from the vertical myoseptum. Consistent with this, the organization of the vertical myosepta, as revealed by the distribution of laminin, dystrophin, and thrombospondin 4b (Figure 6), appeared unaffected in *fro*^{to27c} mutant embryos.

Discussion

Reverse genetic analysis in the mouse suggested a requirement for Myo18B in the organization of cardiomyocyte myofibrils, but a function in skeletal muscle, although anticipated based on the analysis of its expression in C2C12 myoblasts (Ajima *et al.* 2008), has not previously been described. The recent identification of *MYO18B* mutations in patients

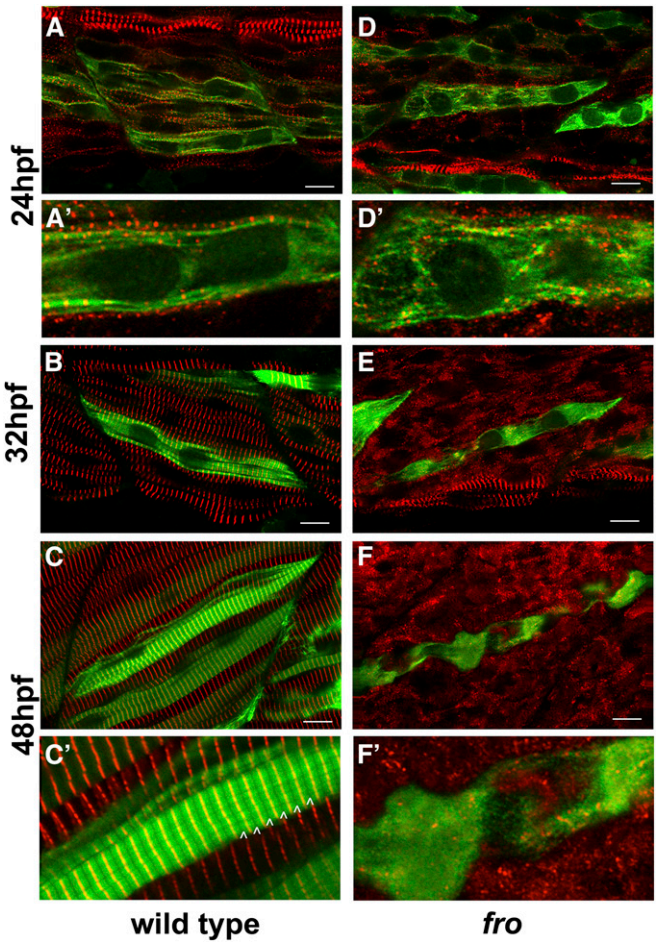

Figure 5 Disruption of myofibrillogenesis in *fro* mutant embryos is first apparent at 24 hfp (hours postfertilization). (A–C) Lateral views of single somites of wild-type embryos transiently expressing Lifeact (green) in individual fast-twitch muscle fibers at successive developmental stages. (A) The accumulation of α-actinin (red) in discrete, regularly spaced puncta along the sarcolemma is first obvious at 24 hpf, as shown in detail in the zoom image (A′); these puncta then expand over the next 24 hr to form the Z-lines (B and C). By 48 hpf, the sarcomeric organization of actin filaments is clearly visible in the zoom image (C′) with the darker M-lines (arrowheads) regularly distributed between the Z-lines. (D) In fro^{to27c} mutants, α-actinin accumulates in irregularly distributed puncta at 24 hpf as shown in the zoom image (D′). At 32 hpf, there is no evidence of Z-lines forming, the α-actinin instead being distributed throughout the cytoplasm (E). This contrasts with the striated distribution in a slow muscle fiber at the bottom of this image. This diffuse distribution persists at 48 hpf with no signs of Z-line formation (F). Similarly, actin is distributed diffusely throughout the fiber with no evidence of sarcomeric organization, as shown in the zoom image (F′). Note that the fibers extend across the width of the somite in the fro^{to27c} mutant embryos. All images are single confocal planes. Bar, 10 μm.

exhibiting symptoms of nemaline myopathy has, however, provided circumstantial evidence for a role of MYO18B in skeletal myogenesis; consistent with this, muscle biopsy analyses revealed defects in sarcomeric organization (Alazami *et al.* 2015; Malfatti *et al.* 2015) reminiscent of those seen in the cardiomyocytes of *Myo18B* mutant mice (Ajima *et al.* 2008).

Our genetic mapping of the zebrafish *fro* mutant to the *myo18b* locus, together with CRISPR/Cas9-mediated targeted mutation of the zebrafish *myo18b* gene, has provided the first definitive evidence of a role for this unconventional myosin in skeletal muscle development and, specifically, in the assembly of the sarcomeres. It is notable that the skeletal muscle phenotype of *fro* mutants appears much stronger than that of the KFA patient muscle, the latter retaining some semblance of sarcomeric organization that is completely lost from the majority of fast-twitch muscle fibers in fish mutant for all four *fro* mutant alleles described here. On the other hand, we found no evidence of the nemaline rods observed in the human patient biopsies and that have previously been described in zebrafish models of nemaline myopathy (Sztal *et al.* 2015). Our analysis has also shown that loss of Myo18B protein results in cardiac defects, arguing against the suggestion that cardiomyopathy associated with the human *MYO18B* mutation is caused by a toxic effect of the truncated mutant protein (Malfatti *et al.* 2015). The effects of *fro* on heart development seem relatively mild compared to the skeletal muscle phenotype: the striated α-actinin distribution suggests some degree of sarcomeric organization and cardiac function, as measured by heart rate appearing to be unaffected. The defects in cardiomyocytes of *Myo18B* mutant mice are similarly mild, sarcomeres of normal length with structures of intercalated disks and Z-lines still being distinguishable (Ajima *et al.* 2008). Sarcomere assembly appeared unaffected in the slow-twitch fibers of *fro* mutants; this is perhaps less surprising given that *myo18b* is not expressed in the slow-twitch muscle lineage. It follows that, although dependent on Myo18B in fast-twitch fibers, sarcomere assembly *per se* does not absolutely require Myo18B function. Whether another unconventional myosin fulfills a similar role to Myo18B in slow-twitch fibers or indeed in cardiomyocytes remains to be determined.

Assembly of sarcomeric units is a complex process that is still not fully understood. One model envisages the polymerization of myosin thick filaments and actin thin filaments in separate multi-protein complexes that subsequently interdigitate to form the sarcomeres (Holtzer *et al.* 1997; Ehler *et al.* 1999). An alternative view is that the process is initiated by the accumulation of α-actinin along the plasma membrane, at integrin-based adhesion sites termed protocostameres, that serves to nucleate the formation of premyofibrils containing nonmuscle myosin II. These premyofibrils subsequently exchange their nonmuscle myosin II for muscle myosin II and extend throughout the fiber (Sparrow and Schock 2009). A recent study in *Drosophila* has highlighted the importance of mechanical tension, generated through the attachment of the growing muscle fibers to tendons, in the assembly of sarcomeres (Weitkunat *et al.* 2014). We see no evidence of defects in the vertical myosepta to which skeletal muscle fibers attach, nor of a failure of attachment of the fast-twitch fibers, arguing against this being a primary cause of myofibrillogenesis failure in *fro* mutants.

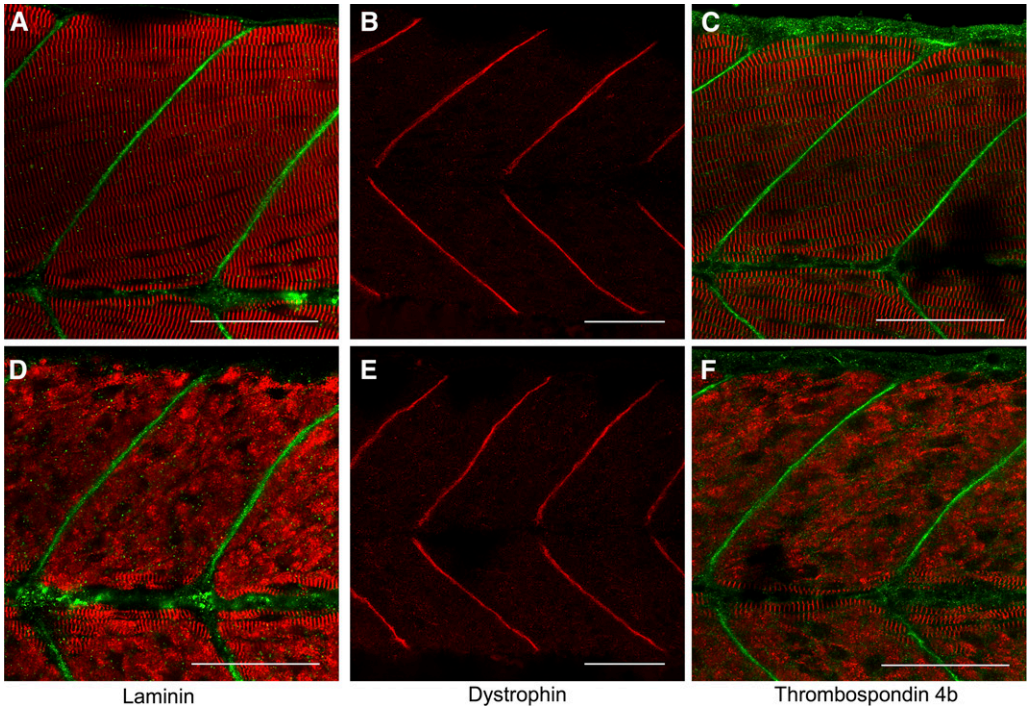

Figure 6 The integrity of the vertical myosepta is unaffected in *fro* mutants. (A–C) Accumulation of laminin (A: green), dystrophin (B: red), and thrombospondin 4b (C; green) marks the vertical myosepta to which muscle fibers, visualized by α-actinin (red) staining in (A) and (C), attach. (D–F) similar images of fro^{to27c} mutant embryos showing that the integrity of the vertical myosepta is unaffected by the loss of Myo18B. All images are single confocal planes of embryos fixed at 48 hpf (hours postfertilization). Bar, 50 μm.

Whereas the formation and attachment of myotubes appears unaffected in *fro* mutants, the accumulation of α-actinin that marks the onset of myofibrillogenesis in wild-type muscle fibers is disrupted from an early stage. In contrast to the regular punctate localization of α-actinin within precursor z-bodies typical of wild-type fast fibers at 24 hpf (Kim and Ingham 2009), α-actinin accumulates in irregularly distributed puncta in *fro* fibers. By 32 hpf, when the z-lines are already well-defined in wild-type fibers, α-actinin is diffusely distributed throughout the cytoplasm of mutant fibers. These findings point to an early role for Myo18B in the assembly of the sarcomeres, but given the paucity of knowledge of the biochemical function of Myo18B, the exact nature of this role remains a matter of speculation. The localization of Myo18B protein to the nucleus of differentiating C2C12 cells has led to the suggestion that it may regulate transcription (Salamon *et al.* 2003; Redowicz 2007); however, its ability to suppress anchorage-independent growth when restored to tumor cells, together with its localization around membrane protuberances and stress fibers (Ajima *et al.* 2007), point rather to a role in regulation of the actin cytoskeleton. Interestingly, the related MYO18A protein, has been implicated in the retrograde flow of the actomyosin network in lamellipodia through its formation of a tripartite complex with LRAP35a and MRCK. In this context, MYO18A is thought to act as an adaptor protein that recruits MRCK, facilitating its phosphorylation of the myosin regulatory light chain (Tan *et al.* 2008). It is tempting to speculate that MYO18B might play a similar role, recruiting other kinases such as ROCK or MLCK, the latter being required for myofibril assembly in cardiomyocytes (Seguchi *et al.* 2007). Further analysis of the *fro* mutant will help shed light on the mechanism of action of this interesting unconventional myosin.

Acknowledgments

We thank C. Nüsslein-Volhard for providing the fro^{to27c} mutant line. We are indebted to Tom Carney for his expert advice and constant input during the course of this study, and to Ed Manser for a helpful discussion about myosin regulation. We thank Tom Schilling for providing the anti-thrombospondin antibody. We are grateful to the staff of the aquaria at the University of Sheffield and the Institute of Molecular and Cell Biology (IMCB), Singapore for zebrafish husbandry. We thank Fiona Chia and Xue Zhi Ouyang for expert technical assistance with the transmission electron microscopy analysis, and Ashley Ng and Weixin Niah for maintaining fish lines. This research project was initially funded by a UK Medical Research Council (MRC) Programme grant (G0100151) and subsequently by core support from the IMCB, the Lee Kong Chian School of Medicine (Nanyang Technological University), and the Living Systems Institute (University of Exeter). P.W.I. gratefully acknowledges the support of the Toh Kian Chui foundation.

Literature Cited

Ajima, R., K. Kajiya, T. Inoue, M. Tani, Y. Shiraishi-Yamaguchi *et al.*, 2007 HOMER2 binds MYO18B and enhances its activity to suppress anchorage independent growth. Biochem. Biophys. Res. Commun. 356: 851–856.

Ajima, R., H. Akazawa, M. Kodama, F. Takeshita, A. Otsuka *et al.*, 2008 Deficiency of Myo18B in mice results in embryonic lethality with cardiac myofibrillar aberrations. Genes Cells 13: 987–999.

Akhmanova, A., and J. A. Hammer, III, 2010 Linking molecular motors to membrane cargo. Curr. Opin. Cell Biol. 22: 479–487.

Alazami, A. M., A. Y. Kentab, E. Faqeih, J. Y. Mohamed, H. Alkhalidi *et al.*, 2015 A novel syndrome of Klippel-Feil anomaly, myopathy, and characteristic facies is linked to a null mutation in MYO18B. J. Med. Genet. 52: 400–404.

Berg, J. S., B. C. Powell, and R. E. Cheney, 2001 A millennial myosin census. Mol. Biol. Cell 12: 780–794.

Ehler, E., B. M. Rothen, S. P. Hammerle, M. Komiyama, and J. C. Perriard, 1999 Myofibrillogenesis in the developing chicken heart: assembly of Z-disk, M-line and the thick filaments. J. Cell Sci. 112(Pt 10): 1529–1539.

Elworthy, S., M. Hargrave, R. Knight, K. Mebus, and P. W. Ingham, 2008 Expression of multiple slow myosin heavy chain genes reveals a diversity of zebrafish slow twitch muscle fibres with differing requirements for Hedgehog and Prdm1 activity. Development 135: 2115–2126.

Granato, M., F. J. van Eeden, U. Schach, T. Trowe, M. Brand *et al.*, 1996 Genes controlling and mediating locomotion behavior of the zebrafish embryo and larva. Development 123: 399–413.

Hawkins, T. A., A. P. Haramis, C. Etard, C. Prodromou, C. K. Vaughan *et al.*, 2008 The ATPase-dependent chaperoning activity of Hsp90a regulates thick filament formation and integration during skeletal muscle myofibrillogenesis. Development 135: 1147–1156.

Heissler, S. M., and J. R. Sellers, 2016 Various themes of myosin regulation. J. Mol. Biol. 428: 1927–1946.

Hernandez, L. P., S. E. Patterson, and S. H. Devoto, 2005 The development of muscle fiber type identity in zebrafish cranial muscles. Anat. Embryol. (Berl.) 209: 323–334.

Holtzer, H., T. Hijikata, Z. X. Lin, Z. Q. Zhang, S. Holtzer *et al.*, 1997 Independent assembly of 1.6 microns long bipolar MHC filaments and I-Z-I bodies. Cell Struct. Funct. 22: 83–93.

Hwang, W. Y., Y. Fu, D. Reyon, M. L. Maeder, S. Q. Tsai *et al.*, 2013 Efficient genome editing in zebrafish using a CRISPR-Cas system. Nat. Biotechnol. 31: 227–229.

Jao, L. E., S. R. Wente, and W. Chen, 2013 Efficient multiplex biallelic zebrafish genome editing using a CRISPR nuclease system. Proc. Natl. Acad. Sci. USA 110: 13904–13909.

Kettleborough, R. N., E. Bruijn, F. Eeden, E. Cuppen, and D. L. Stemple, 2011 High-throughput target-selected gene inactivation in zebrafish. Methods Cell Biol. 104: 121–127.

Kim, H. R., and P. W. Ingham, 2009 The extracellular matrix protein TGFBI promotes myofibril bundling and muscle fibre growth in the zebrafish embryo. Dev. Dyn. 238: 56–65.

Kimmel, C. B., W. W. Ballard, S. R. Kimmel, B. Ullmann, and T. F. Schilling, 1995 Stages of embryonic development of the zebrafish. Dev. Dyn. 203: 253–310.

Knapik, E. W., A. Goodman, M. Ekker, M. Chevrette, J. Delgado *et al.*, 1998 A microsatellite genetic linkage map for zebrafish (*Danio rerio*). Nat. Genet. 18(4): 338–43.

Malfatti, E., J. Böhm, E. Lacène, M. Beuvin, G. Brochier *et al.*, 2015 A premature stop codon in MYO18B is associated with severe nemaline myopathy with cardiomyopathy. J. Neuromuscul. Dis. 2: 219–227.

Nishioka, M., T. Kohno, M. Tani, N. Yanaihara, Y. Tomizawa *et al.*, 2002 MYO18B, a candidate tumor suppressor gene at chromosome 22q12.1, deleted, mutated, and methylated in human lung cancer. Proc. Natl. Acad. Sci. USA 99: 12269–12274.

Odronitz, F., and M. Kollmar, 2007 Drawing the tree of eukaryotic life based on the analysis of 2,269 manually annotated myosins from 328 species. Genome Biol. 8: R196.

Philimonenko, V. V., J. Zhao, S. Iben, H. Dingova, K. Kysela *et al.*, 2004 Nuclear actin and myosin I are required for RNA polymerase I transcription. Nat. Cell Biol. 6: 1165–1172.

Redowicz, M. J., 2007 Unconventional myosins in muscle. Eur. J. Cell Biol. 86: 549–558.

Reischauer, S., O. A. Stone, A. Villasenor, N. Chi, S. W. Jin *et al.*, 2016 Cloche is a bHLH-PAS transcription factor that drives haemato-vascular specification. Nature 535: 294–298.

Riedl, J., A. H. Crevenna, K. Kessenbrock, J. H. Yu, D. Neukirchen *et al.*, 2008 Lifeact: a versatile marker to visualize F-actin. Nat. Methods 5: 605–607.

Salamon, M., C. Millino, A. Raffaello, M. Mongillo, C. Sandri *et al.*, 2003 Human MYO18B, a novel unconventional myosin heavy chain expressed in striated muscles moves into the myonuclei upon differentiation. J. Mol. Biol. 326: 137–149.

Seguchi, O., S. Takashima, S. Yamazaki, M. Asakura, Y. Asano *et al.*, 2007 A cardiac myosin light chain kinase regulates sarcomere assembly in the vertebrate heart. J. Clin. Invest. 117: 2812–2824.

Sparrow, J. C., and F. Schock, 2009 The initial steps of myofibril assembly: integrins pave the way. Nat. Rev. Mol. Cell Biol. 10: 293–298.

Subramanian, A., and T. F. Schilling, 2014 Thrombospondin-4 controls matrix assembly during development and repair of myotendinous junctions. eLife 3: e02372.

Sztal, T. E., M. Zhao, C. Williams, V. Oorschot, A. C. Parslow *et al.*, 2015 Zebrafish models for nemaline myopathy reveal a spectrum of nemaline bodies contributing to reduced muscle function. Acta Neuropathol. 130: 389–406.

Talbot, W. S., and A. F. Schier, 1999 Positional cloning of mutated zebrafish genes. Methods Cell Biol. 60: 259–286.

Tan, I., J. Yong, J. M. Dong, L. Lim, and T. Leung, 2008 A tripartite complex containing MRCK modulates lamellar actomyosin retrograde flow. Cell 135: 123–136.

Vicente-Manzanares, M., X. Ma, R. S. Adelstein, and A. R. Horwitz, 2009 Non-muscle myosin II takes centre stage in cell adhesion and migration. Nat. Rev. Mol. Cell Biol. 10: 778–790.

Vreugde, S., C. Ferrai, A. Miluzio, E. Hauben, P. C. Marchisio *et al.*, 2006 Nuclear myosin VI enhances RNA polymerase II-dependent transcription. Mol. Cell 23: 749–755.

Wallgren-Pettersson, C., C. A. Sewry, K. J. Nowak, and N. G. Laing, 2011 Nemaline myopathies. Semin. Pediatr. Neurol. 18: 230–238.

Wang, X., Y. Ono, S. C. Tan, R. J. Chai, C. Parkin *et al.*, 2011 Prdm1a and miR-499 act sequentially to restrict Sox6 activity to the fast-twitch muscle lineage in the zebrafish embryo. Development 138: 4399–4404.

Weitkunat, M., A. Kaya-Copur, S. W. Grill, and F. Schnorrer, 2014 Tension and force-resistant attachment are essential for myofibrillogenesis in Drosophila flight muscle. Curr. Biol. 24: 705–716.

Communicating editor: M. Halpern